Journal of
Applied
Crystallography

ISSN 1600-5767

Received 5 August 2013
Accepted 4 November 2013

Scanning SAXS–WAXS microscopy on osteoarthritis-affected bone – an age-related study

C. Giannini,[a]* D. Siliqi,[a] M. Ladisa,[a] D. Altamura,[a] A. Diaz,[b] A. Beraudi,[c,d] T. Sibillano,[a] L. De Caro,[a] S. Stea,[c] F. Baruffaldi[c] and O. Bunk[b]

[a]Istituto di Cristallografia (IC-CNR), Via Amendola 122/O, I-70126 Bari, Italy, [b]Paul Scherrer Institut, 5232 Villigen PSI, Switzerland, [c]Laboratorio di Tecnologia Medica, Istituto Ortopedico Rizzoli, Via di Barbiano 1/10, 40136 Bologna, Italy, and [d]Laboratorio PROMETEO-RIT, Istituto Ortopedico Rizzoli, Via di Barbiano 1/10, 40136 Bologna, Italy. Correspondence e-mail: cinzia.giannini@ic.cnr.it

Osteoarthritis (OA), among other bone pathologies, is expected to determine supramolecular changes at the level of the mineralized collagen fiber. In a proof-of-principle study, bone biopsies were collected from six coxarthritis-affected patients, aged 62–87 years, during hip prosthesis implant surgery, sliced down to 100 μm-thick tissues, and investigated using scanning small-angle and wide-angle X-ray scattering (SAXS and WAXS) transmission microscopy. A multimodal imaging evaluation of the SAXS and WAXS data, combined with principal component and canonical correlation analyses, allowed the transformation of the raw data into microscopy images and inspection of the nanoscale structure of the mineralized collagen fibers across mm^2 tissue areas. The combined scanning SAXS and WAXS microscopy is shown to be a suitable choice for characterizing and quantifying the nanostructural properties of collagen over extended areas. The results suggest the existence of a correlation between age and cross-linking-induced rigidity of collagen fibers.

1. Introduction

Primary osteoarthritis (OA) of the hip, also named osteoarthrosis of the hip or coxarthrosis, is a chronic degenerative disorder of the hip joint, causing growing articular pain that can bring the patient to lifestyle limitations until surgical intervention is needed (Hoaglund & Steinbach, 2001). In general, OA of the joints like hip, knee and ankle affects a large part of the elderly population, mostly women, with about 50% of the patients already showing symptoms at the age of 65 (Zhang & Jordan, 2010; Lotz & Loeser, 2012). It is well known that in primary OA the cartilage collagen fibers can become more susceptible to mechanical injury, causing wear and degradation of the articular cartilage (Lotz & Loeser, 2012). At the same time, there is also a significant impact of OA on bone close to the articular cartilage, with important remodeling at the micro scale along the main loading direction of the tissue (Baker-LePain & Lane, 2012). It is important to know if OA affects also the collagen-fiber organization in the articular bone, with attention to the effect of age on bone quality. Any evidence of such a dependence on the age of the patient could lead in the future toward personalized pharmaceutical treatments (Martel-Pelletier *et al.*, 2012) of primary OA, as well as to customized prosthetic devices for joint replacement (Luyten & Vanlauwe, 2012). As an example, therapies aiming at a remineralization of the bone may depend on the collagen structure within the bone being still intact, because the remineralized bone might be very brittle otherwise.

Fundamental questions still have to be addressed about (i) the influence of the patient's age on the quality of the collagen network and the mineral phase in bone, (ii) the existence of a relation between the collagen quality in bone and cartilage, (iii) the parameters promoting natural bone remodeling, and (iv) the influence of pharmaceutical treatments on both the collagen network and the mineral content of the bone.

Small- and wide-angle X-ray scattering (SAXS and WAXS) are established methods which allow the inspection of matter with nanometric or atomic resolution, respectively. Recently, it has been proposed to perform SAXS and WAXS scanning microscopy with a focused X-ray beam to raster-scan a bony tissue specimen (Paris, 2008; Dunlop & Fratzl, 2010; Bünger *et al.*, 2010). This allows nanoscale information to be obtained across mm^2 extended areas.

Such an approach was exploited by the authors of the present article as well, in combination with circularly polarized light (CPL) microscopy, to provide insights on the nanostructure and morphology of cortical and trabecular human bone affected by Paget or dwarfism pathology, at sub-osteon resolution (Giannini *et al.*, 2012).

The aim of the present work has been to collect and analyze SAXS and WAXS scanning microscopies from biopsies of OA-affected bone tissue to investigate possible correlations between age and structural changes at the level of collagen type-I fibers and nanocrystalline hydroxyapatite. Across the investigated samples from a small population of six patients, a

correlation between age and the stiffness of the mineralized collagen fibers, probably cross-linking induced, was found. Indeed, intermolecular cross-linking is a well known natural mechanism preventing the long rod-like collagen molecules from sliding past each other under stress (Bailey *et al.*, 1980). Other authors have found that an excess of cross-links tends to over-stiffen the fibers (Bailey, 2001). Furthermore, for other pathologies or bone conditions, a clear correlation between aging and cross-linking overproduction has been shown (Zimmermann *et al.*, 2011; Saito & Marumo, 2010). The article is organized as follows: a description of the preparation of the bone biopsies and of the setup used to collect SAXS and WAXS data is given in the *Experimental* section; the *Methods* section contains all the steps needed to transform raw data in microscopies; the *Results and discussion* section summarizes the main findings of the work.

2. Experimental

2.1. Patients

The bone specimens in this study were harvested from the femoral necks of six patients, 62–87 years old, during total hip-arthroplasty surgery for primary coxarthrosis. A written informed consent was obtained from the patients. A brief description of the patients in terms of age and gender is reported in Fig. 1.

2.2. Bone sample preparation

Slices of bone 3 mm in height were obtained in the lower area of the femoral neck, always from the same medial sector in proximity to the great trochanter. Once retrieved, the samples were preserved in 4% formalin until being investigated.

Each sample was embedded in methylmethacrylate with its distal surface supported on the container, according to Boyde's method (Boyde *et al.*, 1984; Boyde & Riggs, 1990). In brief, after washing with bidistilled water to remove all the residual marrow debris, the samples were degreased and dehydrated in vacuum with the following series of alcohols: 80% ethanol overnight, 3 steps in 95% ethanol of 1 h each, 5 steps in methanol of 1 h each at 310 K. Infiltration occurred with four passages in methylmethacrylate, first destabilized by chromatography with aluminium oxide and finally embedded in mixtures of methylmethacrylate and di-*n*-butylphthalate at 25%(*w*/*v*) at 298 K. The reaction mixture catalyst was benzoyl peroxide at 3.5%(*v*/*v*).

From the embedded blocks, serial 100 ± 5 µm slices were obtained (Boyde *et al.*, 1984; Boyde & Riggs, 1990) with a 300 µm-thick wafering blade (Leica 1600). The slices were compressed between two glass slides while maintaining the correct orientation. Each slice was visualized in a circularly polarized light microscope (NIKON AZ100 with magnification from 20× to 160×). The CPL data were used to deter-

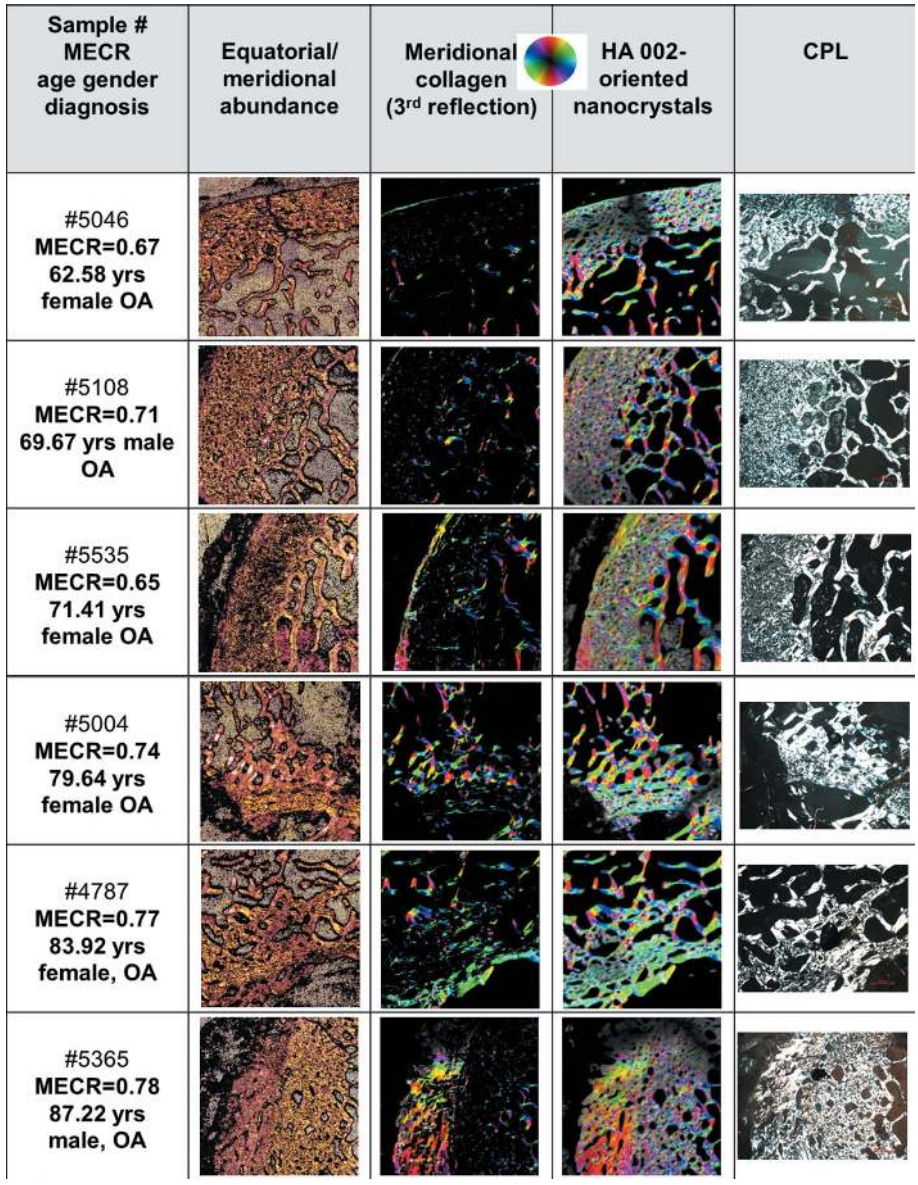

Figure 1
Results of the CCA and multi-modal imaging analysis, compared with the CPL images. Shown are microscopy images of equatorial (yellow) and meridional (magenta) collagen abundance (second column), the collagen meridional scattering monitored *via* the third-order SAXS reflection (third column), the HA(002) WAXS signal (fourth column), and the CPL microscopic images (fifth column). Sample number, age, gender and diagnosis are indicated for each patient, together with the MECR value, namely the ratio between the correlation coefficients of the collagen first-order meridional and equatorial scattering, provided within an error of ±0.02. The color wheel indicates how directions are coded as color in the third and fourth columns.

mine the regions of interest for the scanning SAXS/WAXS microscopy investigations.

2.3. WAXS microscopy

SAXS–WAXS experiments were performed at the cSAXS beamline (Bunk *et al.*, 2009) of the Swiss Light Source (SLS), Paul Scherrer Institut, Villigen, Switzerland, in accordance with all relevant regulations including the Swiss ordinance 814.912 on the contained use of organisms. A monochromatic X-ray beam (E = 13.6 keV) was focused down to about 30 × 30 µm by a bent monochromator crystal and a bent mirror. Each biopsy, 100 ± 5 µm thick, once removed from the glass slides, was placed perpendicular to the direct beam and raster scanned through the beam spot, with the detector measuring the total intensity coming from the currently illuminated spot on the sample, integrated over the exposure time and across the sample thickness. Step sizes of 25 µm in both the horizontal and the vertical direction, and exposure times of 80 ms, were used. The embedding polymer protects the bone biopsy from external contamination as well as from artificial bending, *i.e.* ensures that the X-ray spot illuminates a flat and rigid surface.

To speed up acquisition, data were recorded in a continuous line-scan mode where the sample is moved at constant speed along a line of the two-dimensional raster scan, with the Pilatus 2M detector (Kraft *et al.*, 2009) continuously recording data. SAXS and WAXS data were collected at sample–detector distances of 7092 and 108 mm, respectively. The SAXS and WAXS data sets were transformed into microscopy images as explained in the *Methods* section.

3. Methods

Bone is a composite material whose major components are cross-linked collagen type I, *i.e.* fibrous protein, and nanocrystalline carbonated hydroxyapatite (HA), *i.e.* mineral, which form mineralized fibers assembled in concentric lamellae (Weiner & Wagner, 1998; Rho *et al.*, 2002; Olszta *et al.*, 2007; Dunlop & Fratzl, 2010). Each collagen fiber consists of a staggered arrangement of collagen molecules with embedded HA nanocrystals. Bundles of mineralized collagen fibrils form collagen fibers.

Fig. 2(*a*) shows a schematic drawing of the setup that was adopted in the present experiment to collect the SAXS and WAXS data. In Figs. 2(*b*) and 2(*d*), typical WAXS and SAXS two-dimensional frames are displayed. Fig. 2(*c*) depicts the crystal unit cell for the HA structure that produces the WAXS pattern (Kay *et al.*, 1964), which has been shown here to remind the reader that WAXS data contain information at atomic length scale, like atomic positions, cell symmetry and size.

SAXS is sensitive in general both to nanoscale mineral structures in the size range 1.5–50 nm (Weiner & Wagner, 1998; Rho *et al.*, 2002; Olszta *et al.*, 2007; Dunlop & Fratzl, 2010) and to mesoscale collagen fiber in the size range 65–120 nm (Bigi *et al.*, 1982, Wilkinson & Hukins, 1999; Orgel *et al.*, 2001; Suhonen *et al.*, 2005). The large SAXS sample–detector distance of 7092 mm chosen here allowed us to better resolve mesoscopic length scales. The mesoscale collagen fiber SAXS diffraction pattern is composed of two distinct signals: the meridional and equatorial type-I collagen reflections. The meridional scattering reflections are due to the electron density periodicity along the collagen fiber axis (∼65 nm), the equatorial scattering ones to the packing of the collagen fibrils into fibers (≥100 nm).

Figs. 2(*e*) and 2(*f*) are cartoons of the relative positions of the collagen meridional and equatorial SAXS reflections with respect to the fiber orientation in real space, as expected for a tissue containing type-I collagen fibers. Along with each cartoon, typical corresponding meridional and equatorial SAXS profiles have been reported, to show the link between models and experimental signals. The meridional reflections observed in the SAXS profile of Fig. 2(*e*), located at Δq_1 = 0.0090–0.0119 Å^{-1} (d_1 = 52.9–69.6 nm) and Δq_2 = 0.0274–0.0309 Å^{-1} (d_2 = 20.3–22.9 nm), are diffraction replicas of the $d \simeq$ 64–67 nm periodicities, arising from the packing of the collagen molecules along the fiber axis (Wilkinson & Hukins, 1999; Gentleman *et al.*, 2003). The equatorial profile in Fig. 2(*f*) shows only one broad peak, at about q = 0.0054 Å^{-1}, which corresponds to a length in direct space of about 115 nm, related to the spacing of the collagen fibrils assembled into bundles (Weiner & Wagner, 1998; Suhonen *et al.*, 2005). The higher the degree of packing of fibrils in bundles, the more pronounced and resolved the equatorial reflections are, *i.e.* the greater the inflexibility of the fibrils is, the higher the intensity of the meridional reflections is expected to be.

Lateral structural inhomogeneity in bone tissue is reflected in different collagen SAXS diffraction signals, both meridional and equatorial, as well as in different WAXS signals, across the investigated area. The information encoded in a single SAXS or WAXS two-dimensional frame is averaged over the X-ray-illuminated scattering volume of 30 × 30 × 100 µm in the present case. Inhomogeneity on this or larger length scales can be detected.

Fig. 3 shows four representative two-dimensional/one-dimensional WAXS (Figs. 3*a*–3*d*) and SAXS (Figs. 3*e*–3*h*) frames/patterns simultaneously measured at different sample positions. Figs. 3(*a*) and 3(*e*) present the WAXS and SAXS frames/profiles acquired in an area that does not contain any bone, but only the polymer which embeds the biopsy. The SAXS data vary from an extremely clear and pronounced collagen meridional and equatorial scattering, with up to six–seven meridional diffraction orders (Fig. 3*f*), to an almost isotropically distributed SAXS intensity (Fig. 3*g*), where neither the meridional nor the equatorial peaks are revealed. The intermediate situation of Fig. 3(*h*) shows a case where only the first meridional order is distinguishable from the background and the equatorial scattering is broadly diffused. We selected these four WAXS/SAXS frames/patterns using the principal component analysis (PCA) approach (Abdi & Williams, 2010) as explained below. The intensity anisotropy observed in the SAXS frames depends on the orientation of the collagen fibers in the X-ray-illuminated volume seen in a

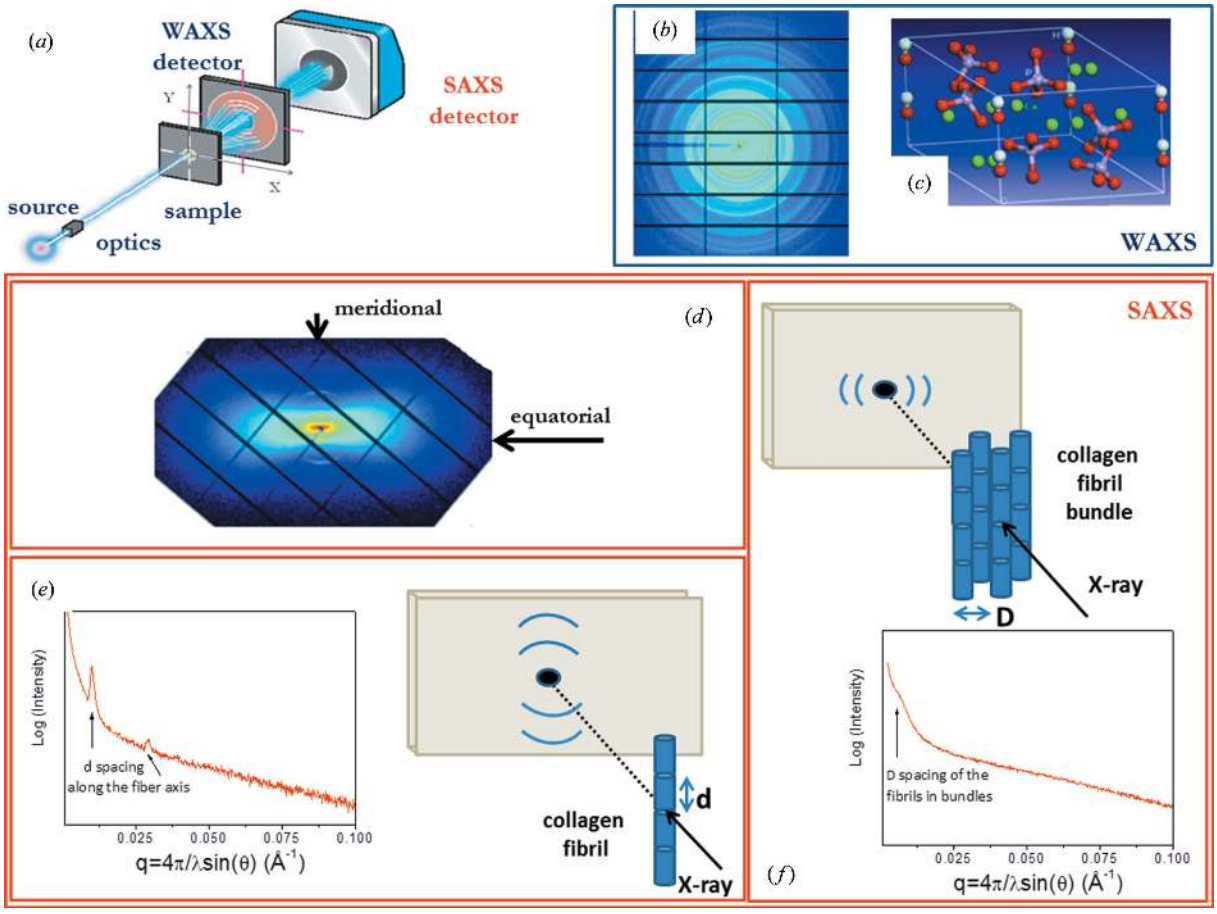

Figure 2
(*a*) A schematic description of the instrumental setup. The X-ray detector is placed at either the short-distance (108 mm, WAXS) or the long-distance (7092 mm, SAXS) position. (*b*) A typical two-dimensional WAXS frame. (*c*) The hydroxyapatite unit cell. (*d*) A typical two-dimensional SAXS frame showing meridional and equatorial reflections. (*e*) and (*f*) The relative orientation of the collagen fibrils and the scattered (meridional and equatorial) intensity peaks (Wilkinson & Hukins, 1999) with the corresponding SAXS experimental patterns. The detector frame in (*d*) has been rotated to match the orientation of the sketches in (*e*) and (*f*).

projection plane perpendicular to the X-ray beam. If the collagen fibers are highly oriented in this plane then an oriented scattering pattern like the one shown in Fig. 3(*f*) will result. If fibers run in different directions within the X-ray-illuminated area in this plane, or if they are oriented mainly along the X-ray beam, then more isotropic scattering patterns will be the result, as in Fig. 3(*g*).

The WAXS frames/patterns displayed in Figs. 3(*b*) and 3(*d*) are typical of data from HA nanocrystals (Giannini *et al.*, 2012) and allow us to attribute the SAXS scattering in Figs. 3(*f*) and 3(*h*) to mineralized collagen fiber, as expected. Conversely, the WAXS data in Fig. 3(*c*) do not correspond to the scattering from the mineral bone component, which allows us to understand why the relevant SAXS data in Fig. 3(*g*) did not contain any reflection related to fiber structure. Most probably, the WAXS/SAXS data in Figs. 3(*c*) and 3(*g*) arise from other types of tissues, different from type-I collagen fiber.

Fig. 4(*a*) is the composite image of a typical scanning SAXS measurement, with each pixel containing a two-dimensional SAXS frame, encoding the strength of the scattering signal from the laterally inhomogeneous sample. The yellow area corresponds to the bone tissue and the blue one to the polymer the biopsy is embedded in. The entire image corresponds to a 7 × 7 mm area of the investigated sample, comprising about 80 000 SAXS frames.

The same area was also studied by WAXS, producing maps analogous to Fig. 4(*a*) (not shown). Considering the large number of SAXS and WAXS two-dimensional frames, data evaluation leading to scanning microscopy images with SAXS or WAXS contrast [like those shown in Figs. 4(*d*)–4(*f*)] relied on statistical methods and was carried out in the following steps: (1) folding the two-dimensional frames into one-dimensional patterns; (2) length scale definition; (3) the multimodal X-ray scattering imaging method; (4) principal component analysis; and (5) canonical correlation analysis. A flow chart is added in the supporting information[1] (Fig. S1) to summarize the logic underneath the analysis.

Let us follow step by step the entire procedure. All two-dimensional SAXS and WAXS frames were azimuthally integrated into one-dimensional profiles (two-dimensional–

[1] Supporting information for this article is available from the IUCr electronic archives (Reference: RG5051).

one-dimensional folding). Typical one-dimensional SAXS and WAXS profiles are presented in Figs. 4(*b*) and 4(*c*), respectively: the SAXS profile showing meridional diffraction peaks, replicas of electron density periodicity along the collagen fiber axis; the WAXS profile being indexed as the diffraction pattern of the hydroxyapatite (HA) crystalline phase, as expected for the mineral bone tissue component (Giannini *et al.*, 2012).

From the SAXS/WAXS profiles (Figs. 4*b* and 4*c*), four peaks, two for the SAXS and two for the WAXS data, were identified as signals to be monitored through the entire raster scan (length scale definition). The peaks correspond to precise length scales: Δq_1 = 0.0090–0.0119 Å^{-1} (d_1 = 52.9–69.6 nm) and Δq_2 = 0.0274–0.0309 Å^{-1} (d_2 = 20.3–22.9 nm), extracted from the SAXS data, corresponding to the first and third meridional reflections of collagen (see Fig. 4*b* and inset) and carrying information on the periodicity along the fiber axis; Δq_3 = 1.8051–1.9061 Å^{-1} (d_3 = 0.330–0.348 nm) and Δq_4 = 2.0358−2.1050 Å^{-1} (d_4 = 0.309–0.299 nm) related to the 002 and 210 crystallographic reflections, respectively, of the HA

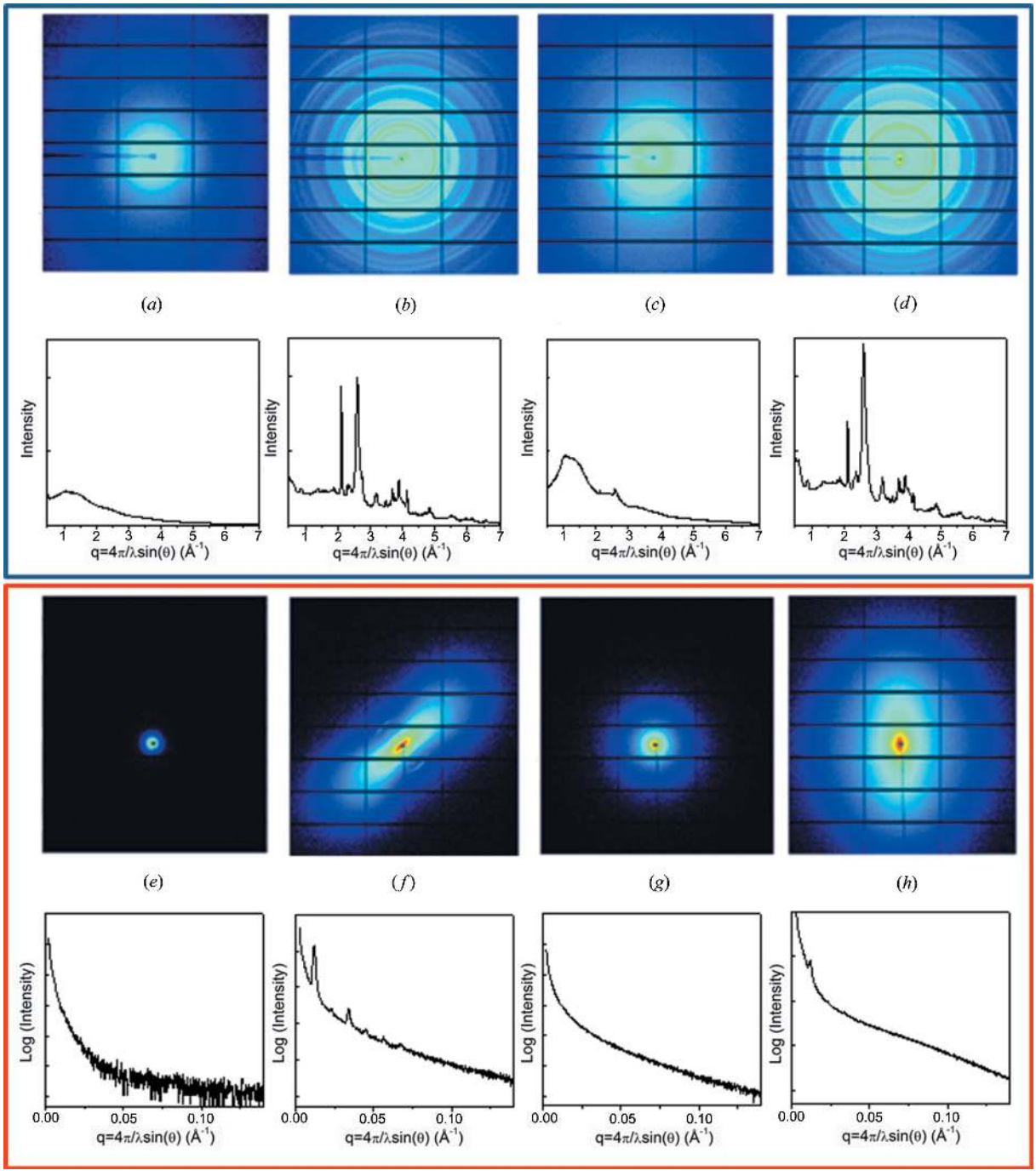

Figure 3
Typical collagen two-dimensional/one-dimensional WAXS frames/patterns (top row) and two-dimensional/one-dimensional SAXS frames/patterns collected on the same sample at different lateral positions.

WAXS pattern (see Fig. 4*c* and corresponding inset) and carrying information on the nanocrystalline hydroxyapatite mineral component of bone. The spacing of the third meridional reflection (d_2) is just a higher-order replica of the first meridional reflection of collagen (d_1), *i.e.* $d_2 = 3d_1$, and they both monitor the same direction and packing along the fiber axis.

Once the length scales of interest had been selected, the final quantitative microscopy images were composed by means of the multi-modal X-ray scattering imaging method (Bunk *et al.*, 2009). Each SAXS/WAXS two-dimensional frame was divided into 16 angular sectors, each 22.5° wide (see also Fig. S1), and only the diffraction rings selected in the previous step were studied from the entire two-dimensional frame. The presence/absence of these diffraction rings, as well as the intensity distribution along the azimuth, was studied, and relevant quantitative information was extracted and transformed into microscopy images (shown in Figs. 4*d*–4*f*). The evaluation of the background below each of the monitored peaks was performed by linear interpolation through three–four selected points on the tails of the WAXS peaks and interpolation of an empirical $10^{-2.6}$ background for the first-order and $10^{-1.5}$ for the third-order collagen peaks in the SAXS data. For the HA 210 peak no background subtraction was applied since it overlaps with a neighboring peak. This leads to an isotropic background in the sample regions where the polymer used for embedding is prominent. The following information was encoded in these images: (i) the local presence (color) or absence (black) of collagen/HA tissue components per pixel, (ii) the orientation of the collagen fibers/HA nanocrystals designated by the direction of the relevant sector within the colored wheel, with white assigned to un-oriented material, and (iii) the degree of orientation of the collagen fibers/HA nanocrystals, determined as the brightness of the colors. The HA orientation is displayed both along the nanocrystal elongation direction, *i.e.* the [002] crystallographic direction, and perpendicular to it, along the [210] direction. A comparison of Figs. 4(*d*) and 4(*e*) immediately confirms that the long axis of the HA nanocrystals is parallel to the collagen fiber axis, as expected from the literature (Paris, 2008; Dunlop & Fratzl, 2010). The orthogonality of the [002] and [210] HA crystal axis orientations in Figs. 4(*e*) and 4(*f*) confirms the reliability of the automated orientation extraction.

As a further step in the statistical analysis of the two-dimensional SAXS/WAXS scanning maps, four representative one-dimensional WAXS patterns were extracted from the whole data set, for each sample, by using a PCA approach, searching for the lowest correlated signals (Abdi & Williams, 2010). The two-dimensional/one-dimensional WAXS frames/

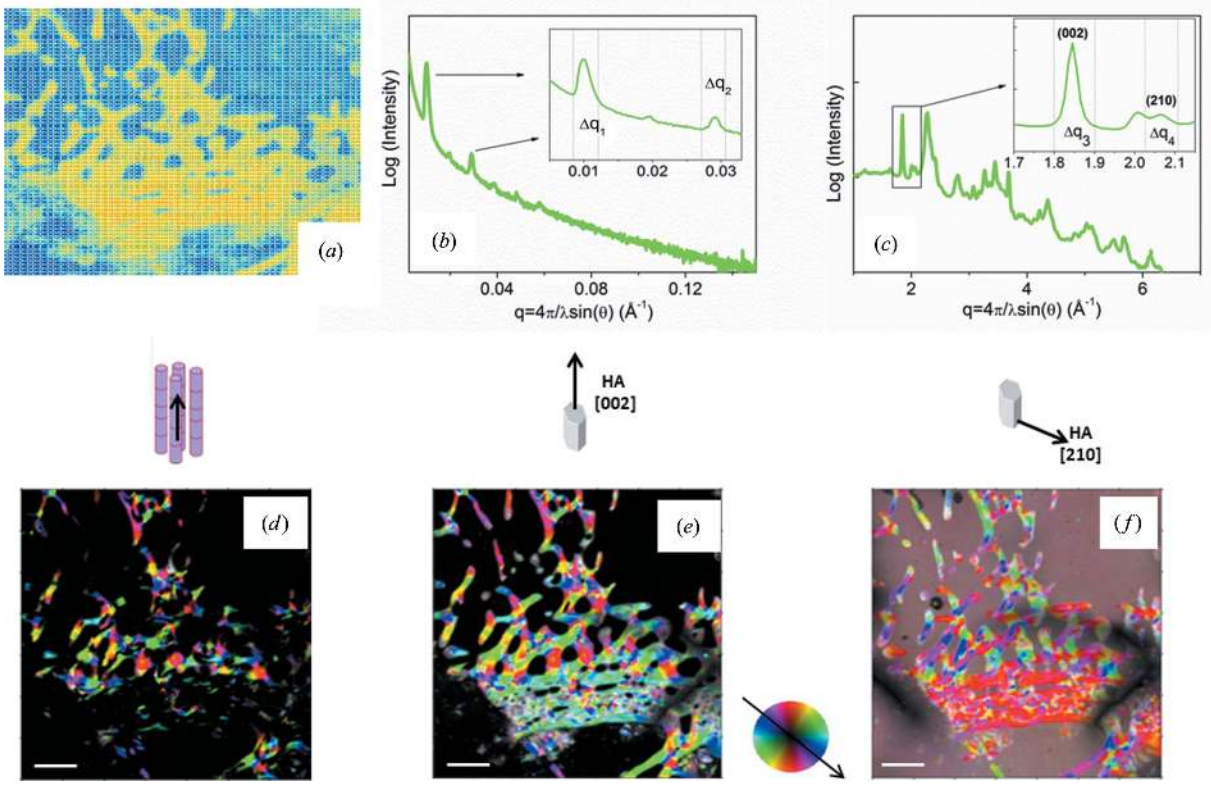

Figure 4
(*a*) A representation of two-dimensional scanning SAXS data, with each pixel containing a two-dimensional SAXS frame. (*b*) An azimuthally integrated SAXS profile, with a zoom on the first meridional reflection of collagen in the inset. (*c*) An azimuthally integrated WAXS profile, with a zoom of the 002 and 210 reflections of HA in the inset. (*d*) Two-dimensional SAXS microscopy mapping the first meridional reflection of collagen at $\Delta q_1 = 0.0090$–0.0119 Å^{-1} (52.9–69.6 nm). (*e*) Two-dimensional WAXS microscopy mapping the 002 peak of the HA component at $\Delta q_3 = 1.8051$–1.9061 Å^{-1} (0.330–348 nm); (*f*) Two-dimensional WAXS microscopy mapping the 210 peak of the HA component at $\Delta q_4 = 2.0358$–2.1050 Å^{-1} (0.309–0.299 nm). The scale bar length in the microscopy images is 1 mm. The color wheel designates the SAXS orientation for each pixel of the maps in (*d*), (*e*) and (*f*).

patterns have already been shown in Figs. 3(*a*)–3(*d*) and coupled to the two-dimensional/one-dimensional SAXS frames/patterns of Figs. 3(*e*)–3(*h*). It is worth specifying that the PCA analysis was applied to one-dimensional WAXS patterns, instead of one-dimensional SAXS, because they contain more quantitative information, *i.e.* more diffraction peaks, readily accessible to a robust model-dependent analysis.

In the last analysis step, considering that each SAXS two-dimensional frame was previously divided into 16 angular sectors, each 22.5° wide, meridional and equatorial scattering profiles were easily identified for each SAXS frame in Figs. 3(*e*)–3(*h*). From them, three main one-dimensional SAXS profiles were taken as model variables in a canonical correlation analysis (CCA) (Laudadio *et al.*, 2005; Ladisa *et al.*, 2007). They are depicted in Fig. 5(*a*) for sample #5004: meridional (magenta), equatorial (yellow) and background profiles (black) have been vertically shifted for the sake of clarity. The CCA is a statistical method which quantifies the relationship between two random variables: the *x* variable (models) representative here of the meridional, equatorial and background profiles; and the *y* variable consisting here of SAXS intensity profiles obtained from the original two-dimensional frames once folded into 16 profiles, one for each 22.5°-wide angular segment (see also Fig. S1). The CCA allows us to quantify the degree of linear dependence between *x* and *y*, providing the so-called correlation coefficient, a scalar quantity with a value between 0 and 1. Through CCA, the contribution of the three major principal signals in Fig. 5(*a*) was determined for each point, and for each sector, of the scanning two-dimensional SAXS image of Fig. 5(*a*) returning 16 nosological maps. In the maps the pixel color is defined by using the CMYK color map: the cyan component is set to zero; magenta represents correlation with the collagen meridional scattering model; yellow, the correlation with the collagen equatorial scattering model; black, the correlation with the background model (Ghersetich *et al.*, 1994). The sector shown in Fig. 5(*b*) was selected, among the 16 available, as one of the nosological maps not dominated by either the equatorial or the meridional signals but with a significant content of information in terms of relative abundance of both.

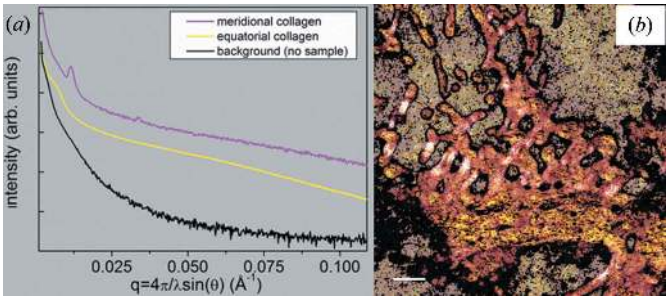

Figure 5
(*a*) Meridional (magenta), equatorial (yellow) and background (black) models. (*b*) CCA nosological map. The meridional and the equatorial components are indicated in magenta and yellow, respectively, using a CMYK color map. The scale bar length in the microscopy image is 1 mm.

The data analysis procedure described in Figs. 3, 4 and 5 was repeated for the entire set of biopsies. The results are summarized in Fig. 1.

4. Results and discussion

The SAXS/WAXS microscopy images provide a full description of the local abundance of collagen fibrils and their HA mineralization.

Fig. 1 summarizes some of the experimental findings: comparing the third-order collagen meridional signal, shown in the third column, with the map of the HA(002) crystals, shown in the fourth column, it is evident that, for all samples, the colors in these images and thereby the orientation of collagen and HA [002] coincide. This confirms both prior findings, namely that the hydroxyapatite [002] crystal direction is aligned with collagen fibers (Paris, 2008; Dunlop & Fratzl, 2010) and the robustness of the data analysis of these two independent measurements.

For verification purposes the collagen first meridional diffraction order SAXS map and the HA [210] WAXS map are also reported in the supporting information in Fig. S2. Here, the colors, *i.e.* orientation, of the first and third collagen map coincide, as expected, since they are caused by the same repeat distance along fibers ($d \simeq 65$ nm = $d_1 = d_2/3$). In the crystallographic structure of HA, the [210] and [002] crystal axes are perpendicular to each other. Comparing the corresponding maps in Fig. S2, their orientation – encoded as color – is perpendicular to each other, demonstrating that we are correctly probing two perpendicular signals from crystals having identical orientation.

The CCA of the SAXS signals reveals the abundance of collagen equatorial scattering (sensitive to the packing of mineralized collagen fibrils in bundles) and collagen meridional scattering (sensitive to the about 65 nm repeat distance occurring along the axis of each fibril/fiber). These two signals are coded as yellow and magenta in the images shown in the second column of Fig. 1. By visual inspection one might get the impression that the CCA images of the samples from younger patients (#5046 and #5108) have a slightly more yellow color than the images for the samples from older patients, which tend more towards magenta. In order to quantify this tendency towards magenta, *i.e.* increased meridional scattering, we computed across the entire CCA map the ratio between the correlation coefficients of the meridional and equatorial scattering, here called the MECR value, which is indicated in Figs. 1 and S2. Each MECR value may vary by about ±0.02 with respect to those segments similar to that represented in Fig. 1, *i.e.* not dominated by any of the equatorial or meridional signals. The derived values are 0.65–0.71 for patients in the age range from 62 to 71 and increase with age up to a maximum of 0.78 for the oldest patient of 87 years. By calculating the correlation coefficient of MECR as a function of age from the data in Fig. 1, an R^2 value equal to 0.77 is found, which is statistically significant at the 5% level (meaning that MECR and age are correlated at a 95% level), pointing towards a linear dependence between MECR and

age. Actually the MECR values reported in Fig. 1 also concide with the median evaluated for each sample on all the 16 sectors. The median is, among the statistical measures of central tendency, the one that most fulfills the property of robustness, with respect to mode or mean, in the presence of anomalous data (Kenney & Keeping, 1962) – which are expected here, at least in the angular sector across the beam stopper.

In elderly individuals, the level of joint immobilization is expected to increase with age. The loss of movement is also concomitant with a decrease in the quantity of water accumulated in the body and with a reduction of glycosaminoglycans, especially hyaluronic acid, in most tissues. These are effects typical of aging (Ghersetich *et al.*, 1994). In other pathologies, it was found that aging produces an increase of the collagen cross-links (Zimmermann *et al.*, 2011; Saito & Marumo, 2010). These increased levels of cross-linking with age stiffen the collagen fibrils, thereby affecting the plasticity of the bone (Zimmermann *et al.*, 2011). How would these changes be manifested at a supra/submolecular level? As already explained, the collagen meridional and equatorial diffraction signals are related to the order along the collagen fibers (meridional) and to the order of the fibril in bundles (equatorial). An increased cross-linking, promoting the stiffening of the fibers, is expected to cause an increased level of the meridional *versus* equatorial scattering signal, as observed in the data. In other words, more rigid fibers allow the scattering signal due to the order along the fiber axis to be more pronounced. In other connective tissues, an increase in the mechanical integrity of the collagen network with age (Wang *et al.*, 2002), which causes much more rigid fibers, loss of elasticity and a consequent brittleness of the bones, was also found.

In conclusion, in spite of having statistically little relevance as collected on a small group of patients, this complex crystallographic study performed with scanning SAXS/WAXS microscopy allowed us to mark a structural variation at the meso/nanoscale with age in OA pathology. The enhancement in the collagen scattering with age was supposed to be related to an increased level of cross-links, inducing stiffening of the collagen fibrils.

The authors would like to thank the SEED project 'X-ray synchrotron class rotating anode microsource for the structural micro imaging of nanomaterials and engineered biotissues (XMI-LAB)', IIT Protocol No. 21537 of 23 November 2009, and the FIRB 2009/2010 project 'Rete integrata per la Nano Medicina (RINAME)', RBAP114AMK_006, and Caterina Chiarella for her support with this project. The authors acknowledge financial support from the European Commission under the Seventh Framework Programme by means of the grant agreement for the Integrated Infrastructure Initiative No. 262348 European Soft Matter Infrastructure (ESMI). Davide De Cristoforo (DDC) and Andreas Menzel are acknowledged for critical reading of the paper and DDC also for fruitful discussions on the OA pathology. Xavier Donath is acknowledged for technical assistance with the measurements at the cSAXS beamline.

References

Abdi, H. & Williams, L. J. (2010). *Comput. Stat.* **2**, 433–459.
Bailey, A. J. (2001). *Mech. Ageing Dev.* **122**, 735–755.
Bailey, A. J., Light, N. D. & Atkins, E. D. (1980). *Nature*, **288**, 408–410.
Baker-LePain, J. C. & Lane, N. E. (2012). *Bone*, **51**, 197–203.
Bigi, A., Ripamonti, A., Roveri, N., Compostella, L., Roncon, L. & Scivazappa, L. (1982). *Int. J. Biol. Macromol.* **43**, 87–92.
Boyde, A., Bianco, P., Portigliatti Barbos, M. & Ascenzi, A. (1984). *Metab. Bone Dis. Relat. Res.* **5**, 299–307.
Boyde, A. & Riggs, C. M. (1990). *Bone*, **11**, 35–39.
Bünger, M. H., Oxlund, H., Hansen, T. K., Sørensen, S., Bibby, B. M., Thomsen, J. S., Langdahl, B. L., Besenbacher, F., Pedersen, J. S. & Birkedal, H. (2010). *Calcif. Tissue Int.* **86**, 294–306.
Bunk, O., Bech, M., Jensen, T. H., Feidenhans'l, R., Binderup, T., Menzel, A. & Pfeiffer, F. (2009). *New J. Phys.* **11**, 123016.
Dunlop, J. W. & Fratzl, P. (2010). *Annu. Rev. Mater. Res.* **40**, 1–24.
Gentleman, E., Lay, A. N., Dickerson, D. A., Nauman, E. A., Livesay, G. A. & Dee, K. C. (2003). *Biomaterials*, **24**, 3805–3813.
Ghersetich, I., Lotti, T., Campanile, G., Grappone, C. & Dini, G. (1994). *Int. J. Dermatol.* **33**, 119–122.
Giannini, C., Siliqi, D., Bunk, O., Beraudi, A., Ladisa, M., Altamura, D., Stea, S. & Baruffaldi, F. (2012). *Sci. Rep.* **2**, 435.
Hoaglund, F. T. & Steinbach, L. S. (2001). *J. Am. Acad. Orthop. Surg.* **9**, 320–327.
Kay, M. I., Young, R. A. & Posner, A. S. (1964). *Nature*, **204**, 1050–1052.
Kenney, J. F. & Keeping, E. S. (1962). *Mathematics of Statistics*, Part 1, 3rd ed., pp. 32–35, 52–54 and 211–212. Princeton: Van Nostrand.
Kraft, P., Bergamaschi, A., Bronnimann, C., Dinapoli, R., Eikenberry, E. F., Graafsma, H., Henrich, B., Johnson, I., Kobas, M., Mozzanica, A., Schleputz, C. M. & Schmitt, B. (2009). *IEEE Trans. Nucl. Sci.* **56**, 758–764.
Ladisa, M., Lamura, A. & Laudadio, T. (2007). *EURASIP. J. Adv. Signal Process.* article 19260.
Laudadio, T., Pels, P., De Lathauwer, L., Van Hecke, P. & Van Huffel, S. (2005). *Magn. Reson. Med.* **54**, 1519–1529.
Lotz, M. & Loeser, R. F. (2012). *Bone*, **51**, 241–248.
Luyten, F. P. & Vanlauwe, J. (2012). *Bone*, **51**, 289–296.
Martel-Pelletier, J., Wildi, L. M. & Pelletier, J. P. (2012). *Bone*, **51**, 297–311.
Olszta, M. J., Cheng, X., Jee, S. S., Kumar, R., Kim, Y. Y., Kaufman, M. J., Elliot, P., Douglas, E. P. & LaGowera, L. B. (2007). *Mater. Sci. Eng. R*, **58**, 77–116.
Orgel, J. P. R. O., Miller, A., Irving, T. C., Fischetti, R. F., Hammersley, A. P. & Wess, T. J. (2001). *Structure*, **9**, 1061–1069.
Paris, O. (2008). *Biointerphases*, **3**, FB16–FB26.
Rho, J. Y., Kuhn-Spearing, L. & Zioupos, P. (2002). *Med. Eng. Phys.* **20**, 92–102.
Saito, M. & Marumo, K. (2010). *Osteoporos Int. Feb.* **21**, 195–214.
Suhonen, H., Fernández, M., Serimaa, R. & Suortti, P. (2005). *Phys. Med. Biol.* **50**, 5401–5416.
Wang, X., Shen, X., Li, X. & Mauli Agrawal, C. (2002). *Bone*, **31**, 1–7.
Weiner, S. & Wagner, H. D. (1998). *Annu. Rev. Mater. Res.* **28**, 271–298.
Wilkinson, S. J. & Hukins, D. W. L. (1999). *Radiat. Phys. Chem.* **56**, 197–204.
Zhang, Y. & Jordan, J. M. (2010). *Clin. Geriatr. Med.* **26**, 355–369.
Zimmermann, E. A., Schaible, E., Bale, H., Barth, H. D., Tang, S. Y., Reichert, P., Busse, B., Alliston, T., Ager, J. W. & Ritchie, R. O. (2011). *Proc. Natl Acad. Sci. USA*, **30** 14416–14421.